

## **FRACTURE STRENGTH AND TIME DEPENDENT PROPERTIES OF 0/90 AND $\pm 55^\circ$ -BRAIDED WEAVE SiC/SiC TYPE-S FIBER COMPOSITES**—C. H. Henager, Jr. (Pacific Northwest National Laboratory)<sup>1</sup>

### **OBJECTIVE**

PNNL has performed mechanical property tests on two types of Hi-Nicalon Type-S fiber SiC/SiC composites for the general purpose of evaluating such composites for control rod guide tube applications in the next generation nuclear power (NGNP) high-temperature gas-cooled reactor design. Such composites are also of great interest for fusion applications as well. The mechanical testing consisted of 4-point bend strength, 4-point single-edge notched bend fracture toughness, and 4-point bend slow crack growth testing on both composites from ambient to 1600°C (1873K). The two composite materials that were tested included a  $\pm 55^\circ$ -braided-weave composite with Type-S fibers inclined at  $55^\circ$  to the principal composite axes to simulate a braided tube architecture and a Type-S 0/90 satin-weave composite as a reference material.

### **SUMMARY**

The use of SiC-reinforced composites for fusion or other nuclear applications will not be restricted to 0/90 aligned fiber applications in all cases. Therefore, it is important to understand the role of fiber orientation in the strength, toughness, and time-dependent strength properties for such materials. The use of high-strength ceramic fibers for composites is predicated on optimizing the strength, fracture resistance, and retained strength in aggressive environments, which argues for the best use of fiber strengths, namely on-axis loading for full load transfer to the high-strength fibers. Evans et al. have developed extensive theoretical treatment of such composites loaded in on-axis orientations [1-3] but relatively few researchers have systematically studied the effects of fiber orientation on composite properties, and none have, to the best of our knowledge, performed any time-dependent testing of off-axis composites.

Although limited work has been performed in off-axis orientations, the research that has been performed gives a solid picture of the effects of such loading on the static strength of composites. Lynch and Evans [4] tested a CMC comprised of Nicalon fibers in a magnesium aluminosilicate (MAS) matrix of boron doped cordierite glass made by Corning Glass. The architecture was a  $[0/90^\circ]_3$  cross-ply structure and the testing was in tension using specimens cut at  $0^\circ$ ,  $30^\circ$ , and  $45^\circ$  to the weave bias. The  $30^\circ$  samples were  $[30/60^\circ]$  in an unbalanced orientation while the  $45^\circ$  samples were  $\pm 45^\circ$  balanced weave. Kawai et al. tested a unidirectional carbon/epoxy laminate fabricated from a prepreg tape P2053-20 at various off-axis angles and matched these results to a Tsai-Hill model prediction [5]. Govaert et al. investigated unidirectional glass fiber/epoxy composites made by filament winding and using a heated epoxy bath [6]. Both of these materials exhibit good matches to predictions based on existing models.

In all cases, both the static strengths and strains to failure are greatly reduced when off-axis loading is performed on these representative composites. The strength reductions and fracture strains are greatly reduced for unidirectional composites dominated by matrix failures but less so for the woven materials dominated by fiber failure. On the other hand, a reduction in strength of about 70% for the CMC materials suggests that off-axis loading, if and when it should occur represents a serious loss of strength concern. For the case considered here, which is an application of woven SiC-based composites for control rod guide tubes, it is not obvious that on-axis loading can be guaranteed for a woven tubular structure. For that reason a study of the strength and time-dependent strength properties of a prototypical woven architecture that was representative of a braided tube design was performed by the US Department of Energy at Pacific Northwest National Labs (PNNL) in conjunction with Idaho National Lab (INL) and Oak Ridge National Lab (ORNL). This research report covers the work that was performed at PNNL that examined static and time-dependent strengths and crack growth rates in both  $[0/90^\circ]$  woven composites tested on-axis and a  $\pm 55^\circ$ -braided weave composite designed to represent a tubular composite architecture. Both materials were made with Hi-Nicalon Type-S fibers in a CVI-SiC matrix.

<sup>1</sup>Pacific Northwest National Laboratory (PNNL) is operated for the U.S. Department of Energy by Battelle Memorial Institute under contract DE-AC06-76RLO-1830.

## PROGRESS AND STATUS

### Introduction

The SiC/SiC materials that were tested at PNNL are 1) a 5-harness satin weave, 8-ply, Hi-Nicalon Type-S fiber composite that was purchased in 2004 from GE Power Systems<sup>2</sup> and 2) A Hypertherm<sup>3</sup> composite purchased in 2006 that is  $\pm 55^\circ$  braided weave, 10-ply plate, Hi-Nicalon Type-S fiber composite. Plan view photographs of these materials are shown in Figure 1, which also reveals a major difference between the two composites as a reduced areal fraction of fibers due to the braided weave as compared to the more compact 5-harness satin weave at 0/90. The 5-harness satin weave 0/90 composite from GE Power Systems was manufactured for PNNL in 2002 with a bulk density of  $2.69 \text{ g/cm}^3$  and 40% nominal fiber volume fraction and was fabricated using isothermal chemical vapor infiltration (ICVI). A 150-nm thick pyrocarbon (PyC) interface was applied to the Type-S fibers prior to ICVI processing. The Hypertherm materials were also made with Type-S Hi-Nicalon fibers but coated with a 150 nm PyC, (100 nm CVI SiC, 20 nm PyC)<sub>4</sub> multi-layer interface applied prior to CVI matrix deposition. These materials had a nominal fiber volume fraction of 30%, a bulk density of  $2.9 \text{ g/cm}^3$ , and a 380- $\mu\text{m}$  thick outer seal coat of SiC. The composite lay-up was 10-ply of nominally  $\pm 45^\circ$  braided tubular weave. PNNL measured the weave angle to be  $\pm 55^\circ$  in the flat plate braided weave material.

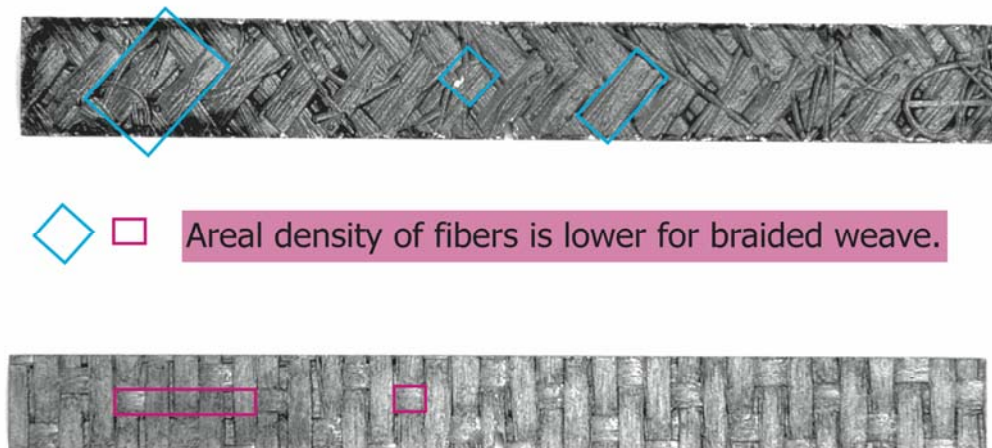


Figure 1. Optical photographs of the two composite materials showing differences in weave architecture and area fraction of fibers. The top image is the  $\pm 55^\circ$  braided weave composite and the bottom image is the 0/90 5-harness satin weave composite material.

### Mechanical property testing

Composite strength, modulus, proportional limit, and ultimate strain were measured for both materials in 4-point bending per ASTM C-1341 (nominal). The typical sample dimensions and bend fixture dimensions are listed in Table 1. The L/d ratios were 19 for the 0/90 composite and 11.1 for the  $\pm 55^\circ$  braid, respectively, which is outside the C-1341 recommended L/d ranges. This might increase the likelihood of shear failures in these materials. The bend data was taken at two strain rates for each material to provide an assessment of slow crack growth in these composites. The 0/90 composite was tested at  $6.7 \times 10^{-6}$  and  $1 \times 10^{-4} \text{ s}^{-1}$  strain rates, while the  $\pm 55^\circ$  braided composite was tested at  $5 \times 10^{-6}$  and  $1 \times 10^{-3} \text{ s}^{-1}$ . The peak load fracture toughness, termed  $K_{Ic}$ , using single-edge notched beams (SENB) of each composite material was determined at ambient temperature and also at elevated temperature based on ASTM C-1421 (see Table 1).

<sup>2</sup><http://www.gepower.com>

<sup>3</sup>Hypertherm HTC Inc. (Huntington Beach, Calif.)

Time-dependent deformation, or slow crack growth, was also measured for both materials. The PNNL technique for determining slow crack growth parameters for the SiC/SiC composites has been to design a test in the spirit of ASTM C-1465 "Determination of Slow Crack Growth Parameters of Advanced Ceramics by Constant Stress-Rate Flexural Testing at Elevated Temperatures" but using a constant load over a range of test temperatures instead of a constant stress rate. For this time-dependent testing either unnotched bend bars or single-edge-notched bars (SENB) can be used to measure deformation rates. The use of SENB bars suggests that crack propagation rates can be determined using standard methods but since multiple matrix cracking is still observed in these materials at the notch, it becomes problematic to analyze the data for crack growth rates, although this has been attempted with some success [7, 8]. A simpler method is to use the deformation rates as measured by mid-point deflections to determine the composite creep parameters by analogy to the fiber creep parameters since, after matrix cracking has occurred, the fibers are carrying the majority of the load on the composite and it is the thermal creep of the highly stressed fibers that determines the deformation rate of the composite. This work features both the use of unnotched bend bars and SENB held at constant load measured over a temperature range given by the results of the strain-rate dependent strength data.

Table 1. Bend and SENB test specifications

Composite Material-Sample	Fixture <sup>4</sup>		Sample <sup>*</sup>		
	Support Span	Loading Span	Span (L)	Depth <sup>5</sup> (d)	Width (W)
0/90 5-harness satin weave – Flexure	40	20	50	2.1	4
±55° braid – Flexure	40	20	50	3.6	4.2
0/90 5-harness satin weave – SENB <sup>6</sup>	40	20	50	5	2.1
±55° braid – SENB <sup>7</sup>	40	20	50	6.1	3.6

<sup>4</sup>All dimensions are in mm in Table 1.

<sup>5</sup>Sample surfaces in depth direction were left as received and were not polished.

<sup>6</sup>a/W values were 0.16 for SENB samples.

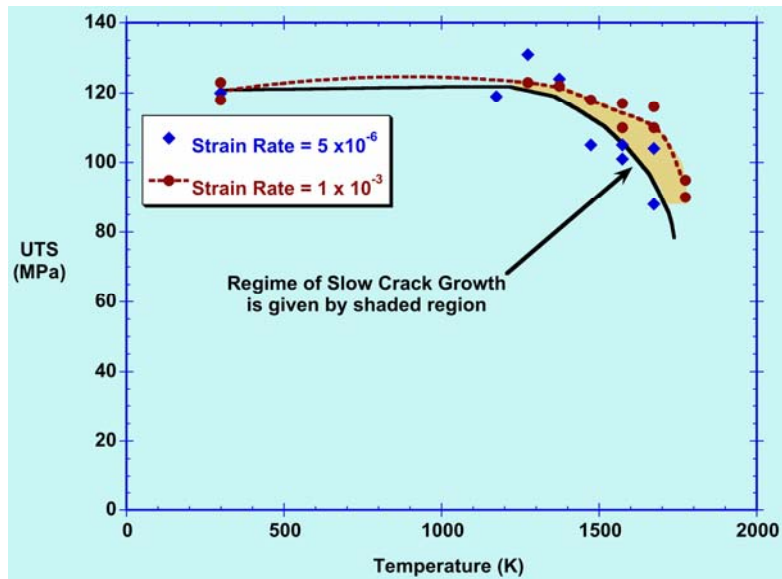
<sup>7</sup>a/W values were 0.16 for SENB samples.

## RESULTS AND DISCUSSION

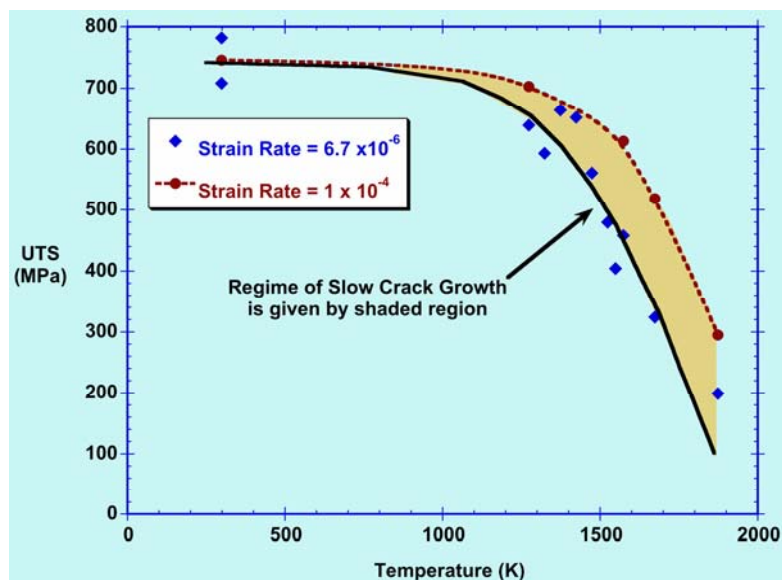
### Rate-dependent bend strength

The bend data are shown in Figure 2 plotted as ultimate bend strength versus temperature for the two strain rates for each material. The difference between the fracture strengths for the fast and slow strain rates is an indication that slow crack growth is occurring in these materials starting at about 1000°C (1273K). The most likely interpretation of this result is that highly strained fibers are undergoing thermal creep at elevated temperatures and failing by creep cavitation [9-23]. The bend data are summarized in Table 2. When compared to the strength of the 0/90 materials it is seen that the braided weave composite has strengths only 15% of the 0/90 material at ambient temperature but about 53% of the 0/90 material at 1600°C. This is an interesting comparison. The lack of strength at ambient temperature appears to be slightly more than can be accounted for by simple fiber geometry

due to the off-axis weave, although modeling this behavior still remains to be done. A survey of the literature reveals that in carbon fiber reinforced plastics a strength reduction of about 80% to 90% for  $\pm 30^\circ$  fiber orientations was observed, while a study of off-axis loaded ceramic composite materials revealed about a 65% strength reduction for  $\pm 30^\circ$  fibers [4, 24]. The lack of sensitivity to elevated temperature strength degradation is likely due to the reduced participation in fiber load sharing relative to the SiC matrix, which is expected to have high resistance to temperature-dependent strength degradation. In other words, the off-axis fiber composite appears to behave more like a monolithic material than a fiber composite and monolithic SiC would exhibit little strength degradation in this temperature range. The high bulk density of  $2.9 \text{ g/cm}^3$  and low fiber volume fraction of 30% could contribute to this result.



(a)



(b)

Figure 2. Ultimate strength (UTS) in bending for (a) Type-S  $\pm 55^\circ$  braided composite at two strain rates and (b) Type-S 5-harness satin weave 0/90 composite at two strain rates.

Table 2. Summary of flexure properties<sup>8</sup>

Composite Material	Temperature (K)	Strength (MPa)	Elastic Modulus (GPa)	Proportional Limit Stress <sup>9</sup> (MPa)	Strain to Failure
0/90 5-harness satin weave	25	740	256	115	.008
	1273	703	223	120	.008
	1573	613	192	110	.007
	1673	519	202	100	.006
	1873	295	182	100	.004
±55° braid	25	120	155	65	.002
	1273	123	178	60	.002
	1573	114	225	45	.0015
	1673	113	246	40	.002
	1873	104	–	–	–

<sup>8</sup>Data taken from fast strain rate tests at elevated temperatures.

<sup>9</sup>Taken from bend stress-strain curve as first deviation from linearity.

### Elastic Modulus in Bending

Representative stress-strain curves in bending are shown in Figure 3 for each type of composite. The linear portion of the initial stress-strain curve was used to compute an elastic modulus in bending for each material, averaging at least two separate stress-strain curves. The 0/90 material has a room temperature modulus of 256 GPa and the ±55° braided weave material has a modulus of 155 GPa as shown in Table 2. Values for the elastic modulus for other temperatures are listed in Table 2.

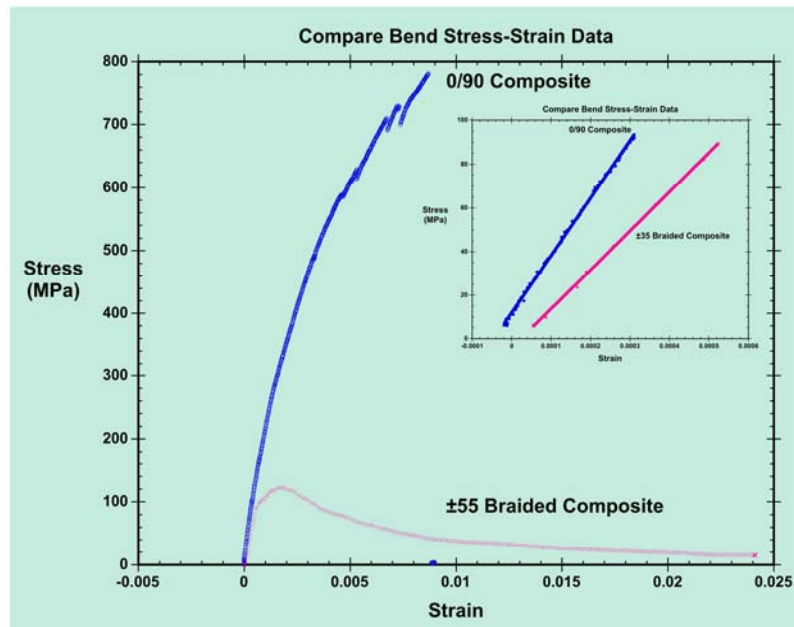


Figure 3. Stress-strain curves in bending for 0/90 and ±55°-braided composite material at ambient temperature. Inset plot shows linear portions of curves used to calculate bending modulus.

### Bend Fracture Photomicrography

Representative fractures are shown in optical micrographs for both 0/90 satin weave and  $\pm 55^\circ$  braided weave materials in Figures 4 to 7. Figure 4 shows typical side views of fractured 0/90 satin weave composite bend bars at the indicated temperature. Some longitudinal splitting along the bar axis is observed and decreasing amounts of fiber pullout are observed with increasing temperature as well as an increased tendency for the fibers to fail within the crack opening region as seen in Figure 5. This pullout length reduction further supports the hypothesis that fibers are failing due to slow crack growth or stress rupture mechanisms. Figure 6 shows similar views for the  $\pm 55^\circ$  braided weave material. Compared to the 0/90 satin weave material the braided weave has less longitudinal splitting during bend testing. Note the 300- $\mu\text{m}$  thick outer layer of SiC on the braided weave material that reduces the fiber volume fraction relative to the 0/90 satin weave material, 30% compared to 40%, respectively. A closer look at the fiber fracture images for the braided weave materials suggests that fibers are failing in bending instead of tension. Figure 7(a) shows broken fibers for the  $\pm 55^\circ$  braided weave material while Figure 7(b) shows broken fibers for 0/90 satin weave material. The fiber fracture surfaces for the braided weave material indicate non-tensile fracture features, while tensile fracture features are readily visible in Figure 7(b) in the form of mirror-mist-hackle regions on the fiber fracture surfaces [25].

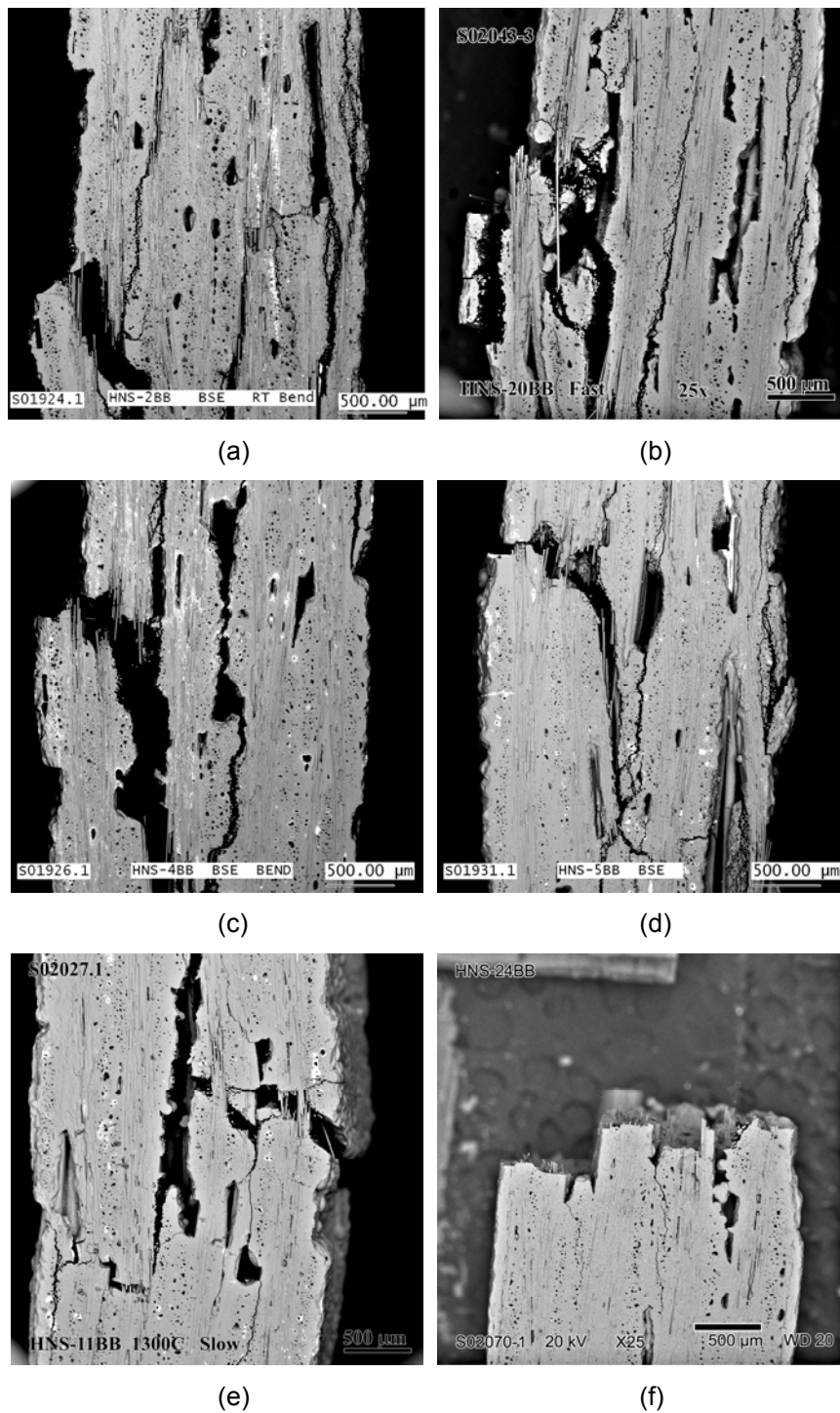


Figure 4. SEM micrographs of bend bars of 0/90 satin weave material after testing in argon at (a) ambient at  $6.7 \times 10^{-6} \text{ s}^{-1}$ , (b) ambient at  $1 \times 10^{-4} \text{ s}^{-1}$ , (c) 1373K at  $6.7 \times 10^{-6} \text{ s}^{-1}$ , (d) 1473K at  $6.7 \times 10^{-6} \text{ s}^{-1}$ , (e) 1573K at  $6.7 \times 10^{-6} \text{ s}^{-1}$ , and (f) 1873K at  $6.7 \times 10^{-6} \text{ s}^{-1}$ .

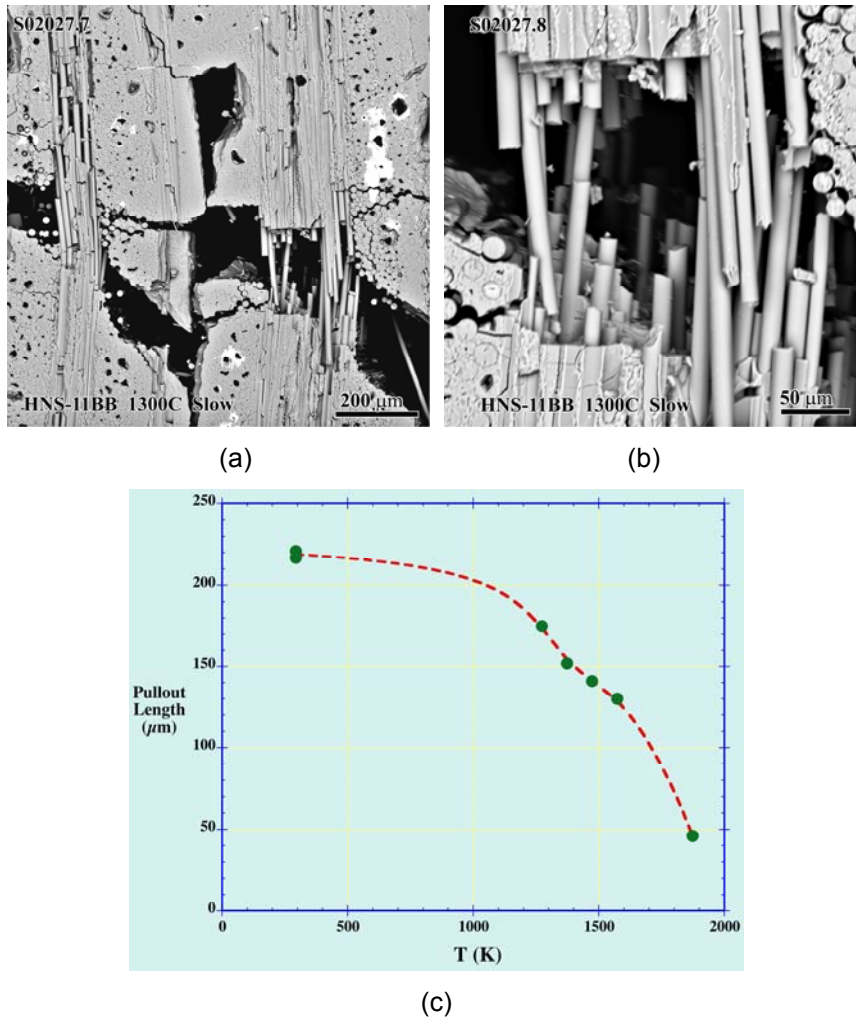


Figure 5. SEM photomicrographs showing fiber failure occurring within the crack opening during bend failure in 0/90 satin weave material at 1573K tested at  $6.7 \times 10^{-6} \text{ s}^{-1}$  in argon in (a) and (b), while in (c) is a plot of fiber pullout lengths as a function of test temperature in argon at  $6.7 \times 10^{-6} \text{ s}^{-1}$ .

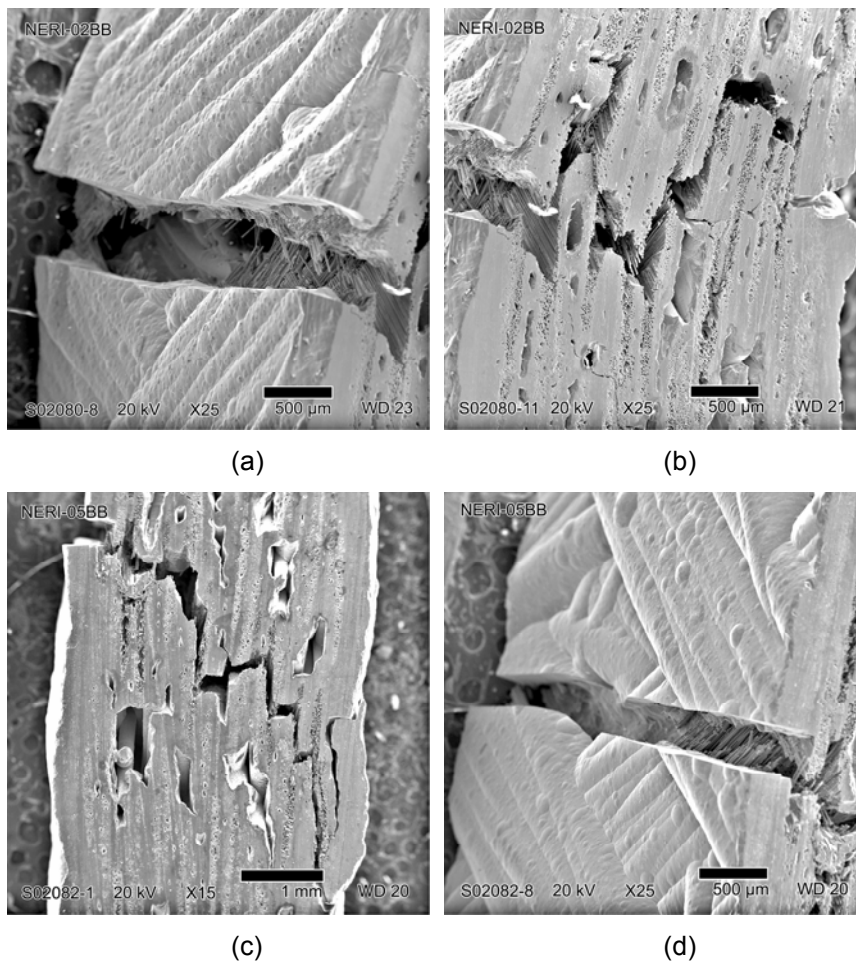


Figure 6. SEM micrographs of bend bars of  $\pm 55^\circ$  braided weave material after testing in argon at (a)-(b) ambient at  $1.0 \times 10^{-3} \text{ s}^{-1}$  and (c)-(d) at 1273K at  $1.0 \times 10^{-3} \text{ s}^{-1}$ .

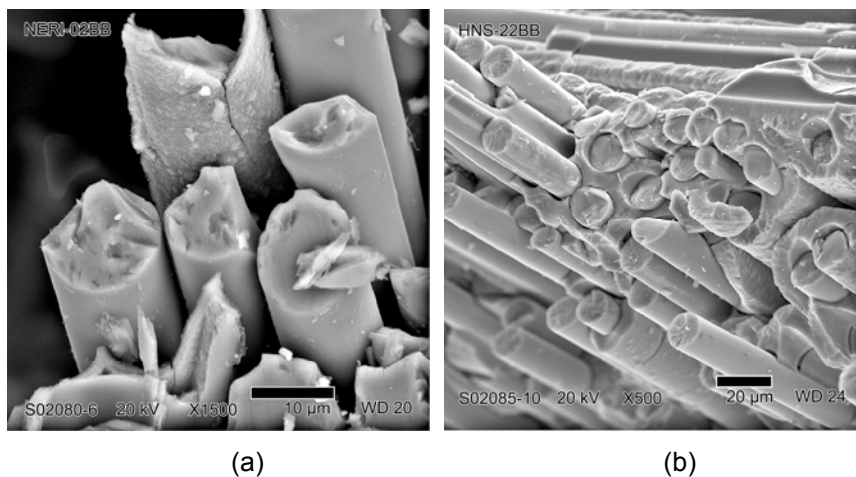
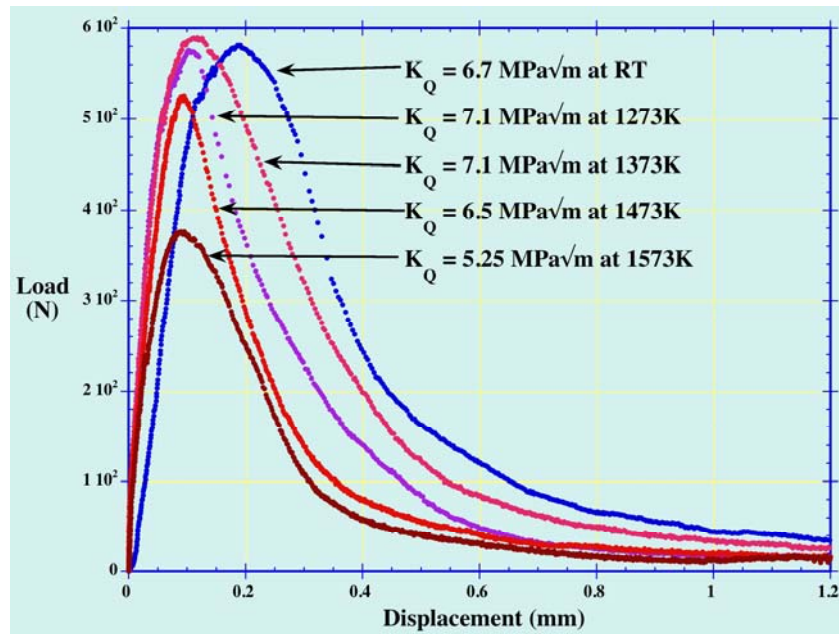


Figure 7. SEM micrographs of failed fibers showing apparent non-tensile fiber failures in (a) for  $\pm 55^\circ$  braided weave materials tested at ambient temperature. In (b) is shown a fracture surface of the 0/90 satin weave material tested at 1673K in argon.

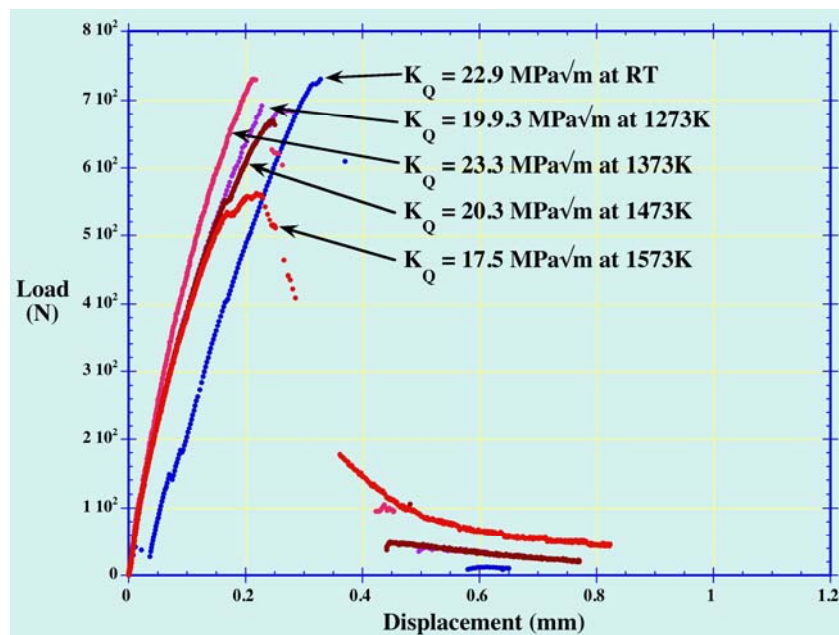
### Fracture Toughness

The room temperature toughness of the  $\pm 55^\circ$ -braided materials was determined to be  $7.7 \text{ MPa}\sqrt{\text{m}}$ ,

which compares to 23 MPa $\sqrt{m}$  for the 0/90 satin weave materials at room temperature. Again, there is a substantial difference of the 0/90 weave versus the  $\pm 55$ -braided weave. Figure 8 shows the peak load curves for both materials as a function of temperature. Toughness values are listed in Table 3.



(a)



(b)

Figure 8. Load-displacement curves for single edge notch beam samples tested at ambient and indicated temperatures. Peak load fracture toughness reported as  $K_Q$  is also indicated.

Table 3. Summary of fracture toughness data

Composite Material	Temperature (K)	Fracture Toughness (MPa√m)
0/90 5-harness satin weave	25	22.9
	1273	19.9
	1373	23.3
	1473	20.3
	1573	17.5
±55° braid	25	7.7 <sup>10</sup>
	1273	7.1
	1373	6.8 <sup>11</sup>
	1473	6.5
	1573	5.25

<sup>10</sup>Average of three tests.

<sup>11</sup>Average of two tests.

### Slow Crack Growth

A type of time-dependent deformation occurs in ceramic composites containing fine-grained or amorphous fibers, such as the Nicalon family of fibers [7, 8, 26]. Composite deformation studies classify these as Type-II composites, which are notch-insensitive materials due to multiple matrix cracking and strong load sharing among fibers. In this case, the SiC-matrix fails in tension by cracking and the load is carried by the Nicalon SiC-fibers, which can then undergo thermal creep deformation at elevated temperatures. The fiber thermal creep process has not been particularly well characterized mechanistically until recently [9, 11] but several groups have performed comprehensive creep studies of the fibers, shown in Table 4, and determined some of the basic creep parameters under either tensile or bending with the bend-stress relaxation technique [9, 10, 21, 23]. A simple characterization of the creep mechanics based on analysis of the best-fit creep equations indicates that fine-grained fiber thermal creep is most likely a grain boundary sliding or viscous flow deformation. This type of deformation is consistent with the low stress exponent and the fractional time-temperature exponent, which typifies a logarithmic creep process that never quite reaches a steady-state process.

The temperature range of interest is determined in this case by the data presented in Figure 2, which shows the temperature region for which time-at-temperature affects the bend strength of the material. For either the 0/90 satin weave or the ±55 braided weave materials this range begins above about 1000°C (1273K) and extends upwards in temperature to the upper use temperature of the material. For the purposes of this study, the upper limit would be established at 1600°C (1873K) but a more practical upper limit is about 1300°C or 1573K since fiber thermal creep is very high at this temperature while the fibers have not started degrading due to thermal processes.

Accordingly, data for the 0/90 satin weave material is shown in Figure 9(a) and that for the ±55 braided weave in Figure 9(b). This data is fit with an equation of the type shown in Table 4 and the subsequent composite time-dependent deformation parameters are determined by curve fitting to the data shown in Figure 9. Comparison of the data with that of the fiber creep data demonstrates the mechanistic similarities that exist and that support the composite fiber creep contention.

This data suggests that the time-dependent deformation characteristics of the 0/90 satin weave and ±55 braided weave materials are similar, which means that the Type-S ceramic fibers are determining the time-dependent deformation of the composites irregardless of their inclination to the crack plane. This finding is supported by the similarity in the time-temperature exponent and activation energies for both materials. It needs to be noted at this point that the loads applied to the ±55 braided weave materials were about one-half of the equivalent loads applied to the 0/90 composite in order to account for their respective fracture toughness levels. This suggests that the PNNL dynamic crack

growth model [7, 8], which has yet to be applied to the inclined fiber composite case, should be able to account for time-dependent crack propagation in the  $\pm 55^\circ$  braided weave composite if the proper geometrical scaling is applied to the crack bridging fibers.

Table 4. Fiber thermal creep and SiC/SiC composite time-dependent data

Fiber type and condition	Creep law <sup>12</sup>	A (MPa <sup>-1</sup> s <sup>-1</sup> )	n	p	Q (kJ/mol)
Nicalon-CG Thermal Creep	$\varepsilon = A \sigma^n t^p \text{Exp}\left(\frac{-Qp}{RT}\right)$	2	1.2	0.4	500 [9, 21]
Hi-Nicalon Thermal Creep	$\varepsilon = A \sigma^n t^p \text{Exp}\left(\frac{-Qp}{RT}\right)$	121	1.8	0.58	445-600 [10, 21]
Type-S Thermal Creep	$\varepsilon = A \sigma^n t^p \text{Exp}\left(\frac{-Qp}{RT}\right)$	0.7	1.0	0.24 – 0.32	500-700 [10]
<b>0/90 Type-S 5-harness satin weave (bend)</b>	$\varepsilon = A' t^p \text{Exp}\left(\frac{-Qp}{RT}\right)$	<b>2090</b> <sup>13</sup>	–	<b>0.33</b>	<b>513</b>
<b><math>\pm 55^\circ</math> Type-S braided weave (SENB)</b>	$\varepsilon = A' t^p \text{Exp}\left(\frac{-Qp}{RT}\right)$	<b>1972</b>	–	<b>0.37</b>	<b>471</b>

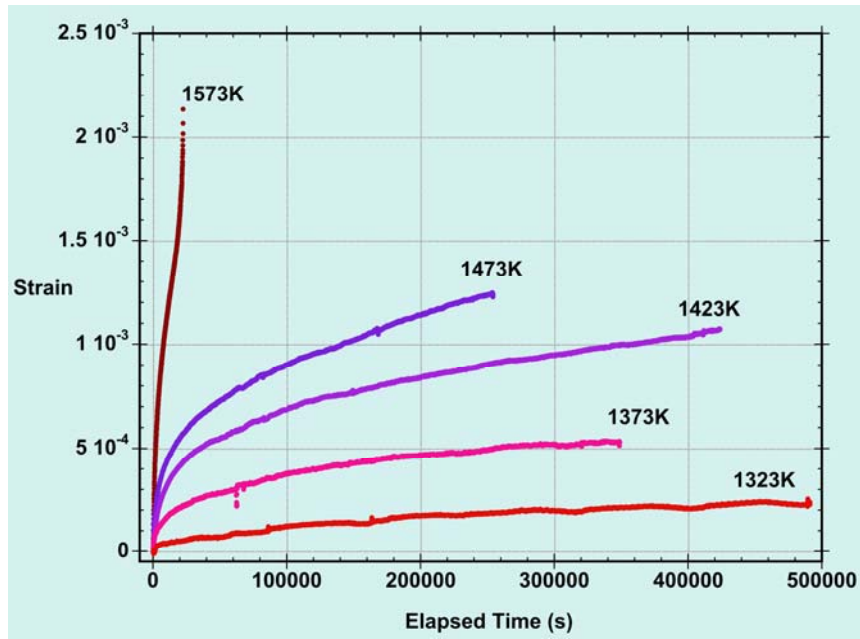
<sup>12</sup>  $s$  is stress in MPa,  $t$  is time in seconds,  $Q$  is activation energy in kJ/mol,  $A$  is a constant, and constants  $n$  and  $p$  are stress and time-temperature exponents, respectively.

<sup>13</sup>  $A'$  combines  $A s^n$  for composites since a constant load was used.

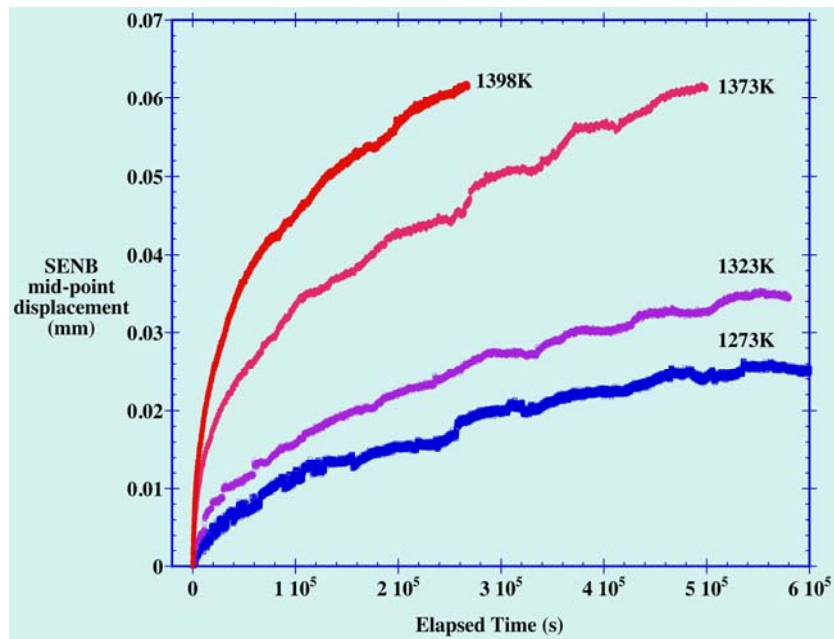
### Inclined Fiber Bridging

anical properties between the 0/90 satin weave and  $\pm 55^\circ$  braided weave materials indicates strength, toughness, and, fracture surface feature differences, but similar slow crack growth mechanisms. Figure 10 shows the differences observed in bend strength between the two materials as a function of test temperature. Although there are substantial differences in fiber volume fraction and outer seal coat thickness between the two materials that partly account for these differences, one major distinction is that fibers are inclined to the principal axes for the  $\pm 55^\circ$  braided weave materials, which acts to reduce fiber load carrying capability, either through decreased strain to failure or other geometrical strength effects. Several researchers have explored mechanics models of such inclined fibers [27-31] and their main findings are summarized here along with an attempt to model the load-displacement curve for an individual inclined fiber in a ceramic matrix for future inclusion into the PNNL dynamic crack bridging model.

Two important issues emerge from this analysis of inclined fibers; first that an additional frictional energy term, so-called snubbing friction, occurs in this problem as the fiber is pulled out and bent near the matrix crack plane [27]. This causes a high friction much as a rope pulled over a curved edge might experience. Second, the matrix acts as an elastic foundation for fiber bending, which modifies conventional bending mechanics in a complex manner, but this problem has been addressed by solid mechanics solutions [30].



(a)



(b)

Figure 9. Strain-time and displacement-time curves for 0/90 satin weave and  $\pm 55$  braided weave materials at constant load. Shown in (a) are the strain-time plots for 0/90 5-harness satin weave bend bars under constant load for the indicated times, and in (b) are the displacement-time plots for SENB samples held at a load that corresponded to an initial  $K_{\text{applied}}$  of  $5 \text{ MPa}\sqrt{\text{m}}$  for the indicated time.

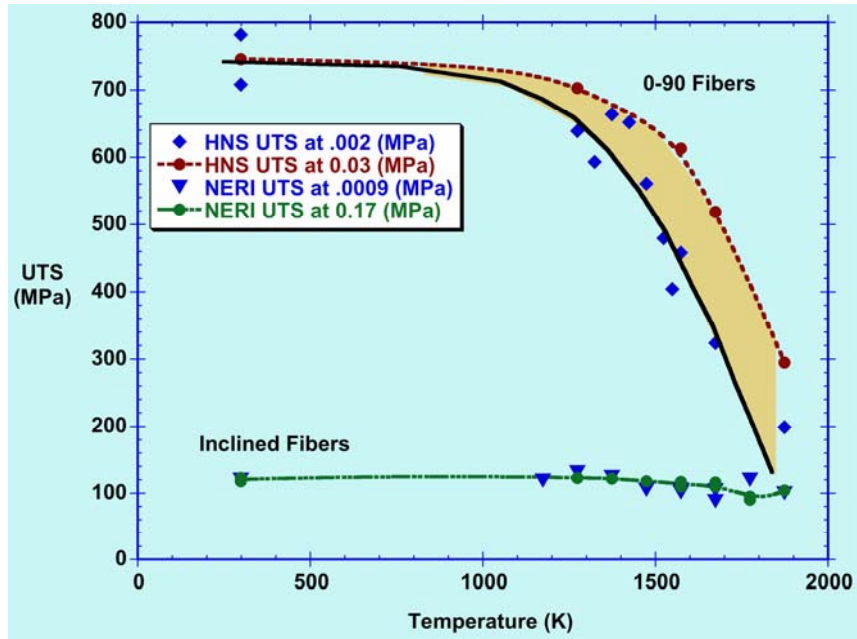


Figure 10. This plot shows the relative strength at ambient temperature and the decrease of strength with test temperature for both composite materials. The  $\pm 55^\circ$  braided weave material has a bend strength of only 15% of the 0/90 satin weave material at ambient temperature but this strength difference decreases at elevated temperatures due to enhanced fiber failure seen in the 0/90 composite.

The work of Cox is taken as a starting point for the representation of an inclined fiber in an elastic matrix and snubbing friction is included in the analysis [27]. The force-displacement solution to an inclined bridging fiber is given as two terms, using normalized variables, as

$$W = \frac{\mu_e \left[ -\cos\phi + \cos(\theta_0 + \phi) + \frac{P \left( \frac{-P \cos\phi + e^{-\frac{\theta_0 \mu_e}{P}} (P \cos\phi - \mu_e \sin\phi)}{\mu_e} + \sin(\theta_0 + \phi) \right)}{\mu_e} \right]}{(P^2 + \mu_e^2) \tau_1} \quad (1)$$

where  $W$  is the fiber deflection,  $P$  is the force,  $\phi$  is the inclination angle,  $\theta_0$  is the bending angle,  $\mu_e$  is the snubbing friction term, and  $\tau_1$  is the conventional sliding friction term. This equation includes the elastic stretch of the inclined fiber as well as the deformation of the inclined fiber across an interface, such as a crack, due to local bending. The resulting force displacement law is compared to that of a fiber oriented normal to the crack plane using a standard shear-lag fiber model in Figure 11. The Cox inclined bridging law was first calibrated normal to the crack plane to match the Marshall-Cox-Evans law [3] and then angle  $\phi$  was changed to  $35^\circ$ . This plot shows the displacement for an inclined fiber relative to a normal bridging fiber as a function of applied force. This result indicates that an inclined fiber will be stiffer relative to the normal fiber, thus the composite energy absorption, strength, and toughness will be proportionally reduced because the inclined fibers will fracture sooner than the normal fibers since the inclined fibers cannot tolerate as much crack opening displacement.

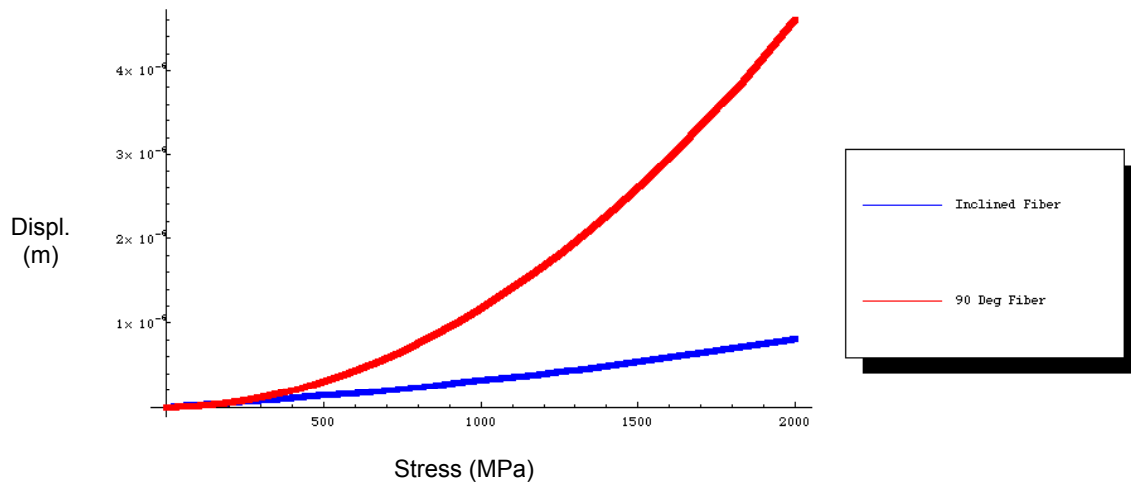


Figure 11. Comparison of stress-displacement laws for an inclined fiber and a normal fiber showing that the inclined fiber appears stiffer relative to the normal fiber. The angle of inclination was set to  $90^\circ - 55^\circ = 35^\circ$  to match the definition of  $\phi$  in Reference [16].

The existence of matrix constraint and snubbing friction suggests that inclined fibers may show telltale fracture surface features of matrix spallation and/or bending failure near the matrix. In Figure 12 indications of this is shown in several SEM micrographs of composite fracture surface features. Figure 12(a) shows slight matrix spallation around a fracture fiber in the 0/90 satin weave material while in Figure 12(b)-(d) much larger regions of matrix spallation can be observed near the inclined fibers in the  $\pm 55^\circ$  braided weave material. The inclined fibers also appear to have failed in bending near the region of matrix egress as non-tensile fracture surface features are observed on the fiber fractures. Although not conclusive evidence of the importance of matrix constraint in this problem, these observations substantiate the analysis of Cox and others that such constraints are important considerations in the fracture of inclined fiber composites.

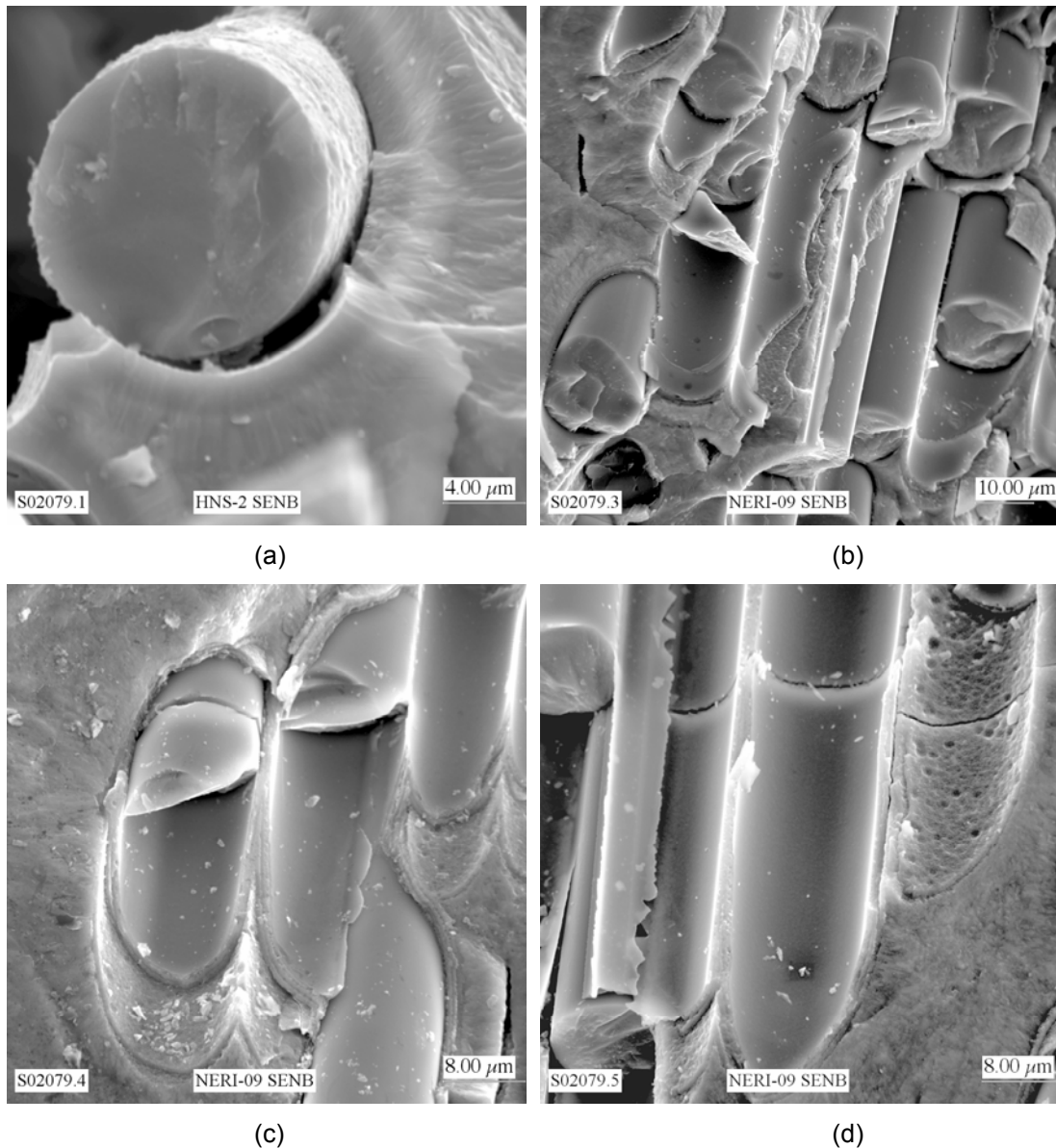


Figure 12. SEM micrographs of composite fracture surfaces showing fiber-matrix constraint and matrix spallation during fracture. In (a) some slight matrix spallation is observed in a 0/90 satin weave material, and in (b)-(d) much larger regions of matrix spallation due to inclined fibers and matrix constraint are observed in  $\pm 55^\circ$  braided weave materials. Note also in (b)-(d) that fibers appear to have failed in bending near matrix egress.

### Conclusions

- The following main points summarize the findings of this work: The  $\pm 55^\circ$  braided weave material exhibited only 15% of the average strength and only 30% of the fracture toughness of the 0/90 composite at ambient temperature. These reductions in strength and toughness were greater than typical reductions observed by others for off-axis fiber composites [4-6].
- Both composites were observed to undergo slow crack growth at elevated temperatures with similar activation energies and time-temperature exponents that are consistent with thermal creep of the Type-S bridging fibers.

- The  $\pm 55^\circ$  braided weave composite with inclined fibers exhibited fiber fractures and fracture surface features consistent with fibers failing due to bending rather than tension and showing evidence of matrix spallation and snubbing friction effects in the plane of bridged cracks.
- The fiber inclination reduced the fiber participation in energy absorption for the  $\pm 55^\circ$  braided weave composite so that it behaved more like a monolithic SiC material compared to the 0/90 composite. This was partly due to composite architectural effects, partly due to fiber inclination, and partly due to non-optimized composite fabrication. The fiber volume fraction was too low and the outer SiC seal coat was too thick.
- The upper use temperature of a Type-S SiC/SiC composite material, regardless of fiber orientation, is limited to about 1300°C (1573K) due to slow crack growth processes and loss of fiber strength at higher temperatures. This study also documented loss of fracture toughness at and above this temperature.
- Preliminary models of inclined fibers bridging cracks in composites show that inclined fiber bridging must include snubbing friction and fiber bending in addition to elastic stretch. Inclined fibers appear “stiffer” in computed force-displacement laws compared to aligned fibers due to some of these factors.

## References

- [1] B. Budiansky, A. G. Evans, and J. W. Hutchinson, *Int. J. Solids Struct.* 32 (1995) 315.
- [2] A. G. Evans and F. W. Zok, *J. Mater. Sci.* 29 (1994) 3857.
- [3] D. B. Marshall, B. N. Cox, and A. G. Evans, *Acta Metall.* 33 (1985) 2013.
- [4] C. S. Lynch and A. G. Evans, *J. Am. Ceram. Soc.* 79 (1996) 3113.
- [5] M. Kawai, Y. Masuko, and T. Sagawa, *Compos. Part A: Appl. Sci. Manuf.* 37 (2006) 257.
- [6] L. E. Govaert, H. J. Schellens, H. J. M. Thomassen, R. J. M. Smit, L. Terzoli, and T. Peijs, *Compos. Part A: Appl. Sci. Manuf. (Incorporating Composites and Composites Manufacturing)* 32 (2001) 1697.
- [7] C. H. Henager, C. A. Lewinsohn, and R. H. Jones, *Acta Mater.* 49 (2001) 3727.
- [8] C. H. Henager, Jr., and R. G. Hoagland, *Acta Mater.* 49 (2001) 3739.
- [9] J. J. Sha, J. S. Park, T. Hinoki, and A. Kohyama, *Mech. Mater.* 39 (2007) 175.
- [10] J. J. Sha, J. S. Park, T. Hinoki, and A. Kohyama, *Mater. Charact.* 57 (2006) 6.
- [11] J. A. DiCarlo, H. M. Yun, and J. B. Hurst, *Appl. Math. Comput. (New York)* 152 (2004) 473.
- [12] J. A. DiCarlo and H. M. Yun, in *Creep Deformation: Fundamentals and Applications (Proceedings of a Symposium held during the 2002 TMS Annual Meeting)*, R. S. Mishra, J. C. Earthman, S. V. Raj (eds.) (Minerals, Metals & Materials Society, Warrendale, Pa., 2002) 195.
- [13] H. M. Yun and J. A. DiCarlo, *Ceram. Eng. Sci. Proc.* 20 (1999) 259.
- [14] J. A. DiCarlo and H. M. Yun, *Adv. Sci. Technol.* 22 (Advanced Structural Fiber Composites) 29 (1999).
- [15] J. A. DiCarlo and H. M. Yun, *Ceram. Trans.* 99 (1998) 119.
- [16] J. C. Goldsby, H. M. Yun, and J. A. DiCarlo, *Scr. Mater.* 37 (1997) 299.
- [17] J. A. DiCarlo, *Ceram. Int.* 23 (1997) 283.
- [18] R. Bodet and J. Lamon, *Silic. Ind.* 61 (1996) 23.
- [19] H. M. Yun, J. C. Goldsby, and J. A. DiCarlo, *Ceram. Trans.* 58 (1995) 331.
- [20] R. E. Tressler and J. A. DiCarlo, *Ceram. Trans.* 57 (1995) 141.
- [21] J. A. DiCarlo, H. M. Yun, G. N. Morscher, and J. C. Goldsby, *Ceram. Trans.* 58 (High-Temperature Ceramic-Matrix Composites II) 343 (1995).
- [22] H. M. Yun, J. C. Goldsby, and J. A. DiCarlo, *Ceram. Trans.* 46 (1994) 17.
- [23] J. A. DiCarlo, *Compos. Sci. Technol.* 51 (1994) 213.
- [24] M. Kawai and T. Taniguchi, *Compos. Part A: Appl. Sci. Manuf.* 37 (2006) 243.
- [25] N. Lissart and J. Lamon, *Acta Mater.* 45 (1997) 1025.
- [26] R. H. Jones and C. H. Henager, Jr., *J. Eur. Ceram. Soc.* 25 (2005) 1717.
- [27] B. N. Cox, *Mech. Adv. Mater. Struct.* 12 (2005) 85.

- [28] D. D. R. Cartie, B. N. Cox, and N. A. Fleck, *Compos. Part A: Appl. Sci. Manuf.* 35 (2004) 1325.
- [29] W. B. Hillig, *J. Mater. Sci.* 29 (1994) 419.
- [30] W. B. Hillig, *J. Mater. Sci.* 29 (1994) 899.
- [31] C. K. Y. Leung and V. C. Li, *J. Mech. Phys. Solids* 40 (1992) 1333.